

## **EXHIBIT D**

# Crystal Structure of the *Aequorea victoria* Green Fluorescent Protein

Mats Ormö, Andrew B. Cubitt, Karen Kallio, Larry A. Gross,  
Roger Y. Tsien,\* S. James Remington†

The green fluorescent protein (GFP) from the Pacific Northwest jellyfish *Aequorea victoria* has generated intense interest as a marker for gene expression and localization of gene products. The chromophore, resulting from the spontaneous cyclization and oxidation of the sequence -Ser<sup>65</sup> (or Thr<sup>65</sup>)-Tyr<sup>66</sup>-Gly<sup>67</sup>-, requires the native protein fold for both formation and fluorescence emission. The structure of Trp<sup>65</sup> GFP has been determined at 1.9 angstrom resolution. The protein fold consists of an 11-stranded  $\beta$  barrel with a coaxial helix, with the chromophore forming from the central helix. Directed mutagenesis of one residue adjacent to the chromophore, Thr<sup>203</sup>, to Tyr or His results in significantly red-shifted excitation and emission maxima.

Although the GFP of the Pacific Northwest jellyfish *Aequorea victoria* was discovered some time ago (1), the cloning (2) and heterologous expression (3) of its cDNA were the crucial steps that triggered the widespread and growing use of GFP as a reporter for gene expression and protein localization in a broad variety of organisms (4, 5). Wild-type GFP is a stable, proteolytically-resistant single chain of 238 residues and has two absorption maxima at about 395 and 475 nm. The relative amplitudes of these two peaks are sensitive to environmental factors (6) and illumination history (4), presumably reflecting two or more ground states. Excitation at the primary absorption peak of 395 nm yields an emission maximum at 508 nm with a quantum yield of 0.72 to 0.85 (1, 4–6). The fluorescence results from the autocatalytic cyclization of the polypeptide backbone between residues Ser<sup>65</sup> and Gly<sup>67</sup> and oxidation of the  $\alpha$ - $\beta$  bond of Tyr<sup>66</sup> (4, 7, 8). Mutation of Ser<sup>65</sup> to Thr (S65T) (9) simplifies the excitation spectrum to a single peak at 488 nm of enhanced amplitude (10), which no longer shows signs of conformational isomers (4). As a step in understanding these properties, and to aid in the tailoring of GFPs with altered characteristics, we have determined the three-dimensional structure at 1.9 Å resolution of the S65T mutant (10) of *A. victoria* GFP (11).

The structure of GFP was determined by multiple isomorphous replacement and anomalous scattering (11) (Table 1), solvent flattening, phase combination, and crystallographic refinement. The most distinctive feature of the fold of GFP is an 11-stranded  $\beta$  barrel wrapped around a single central helix (Fig. 1, A and B), where each strand consists of approximately 9 to 13 residues. The barrel forms a nearly perfect cylinder 42 Å long and 24 Å in diameter. The NH<sub>2</sub>-terminal half of the polypeptide comprises three antiparallel strands, the central helix, and then another three antiparallel strands, the third of which (residues 118 to 123) is parallel to the NH<sub>2</sub>-terminal strand (residues 11 to 23). The polypeptide backbone then crosses the "bottom" of the molecule to form the second half of the barrel in a five-strand Greek key motif. The top end of the cylinder is capped by three short, distorted helical segments, and one

multiple isomorphous replacement and anomalous scattering (11) (Table 1), solvent flattening, phase combination, and crystallographic refinement. The most distinctive feature of the fold of GFP is an 11-stranded  $\beta$  barrel wrapped around a single central helix (Fig. 1, A and B), where each strand consists of approximately 9 to 13 residues. The barrel forms a nearly perfect cylinder 42 Å long and 24 Å in diameter. The NH<sub>2</sub>-terminal half of the polypeptide comprises three antiparallel strands, the central helix, and then another three antiparallel strands, the third of which (residues 118 to 123) is parallel to the NH<sub>2</sub>-terminal strand (residues 11 to 23). The polypeptide backbone then crosses the "bottom" of the molecule to form the second half of the barrel in a five-strand Greek key motif. The top end of the cylinder is capped by three short, distorted helical segments, and one

short, very distorted helical segment caps the bottom of the cylinder. The main chain hydrogen bonding lacking the surface of the cylinder likely accounts for the unusual stability of the protein toward denaturation and proteolysis. There are no large segments of the polypeptide that could be excised while preserving the intactness of the shell around the chromophore. Thus, it would seem difficult to re-engineer GFP to reduce its molecular size (12) by a large percentage.

The *p*-hydroxybenzylideneimidazolidinone chromophore (7) is completely protected from bulk solvent and is centrally located in the molecule. The total and presumably rigid encapsulation is probably responsible for the small Stokes' shift (that is, wavelength difference between excitation and emission maxima), high quantum yield of fluorescence, inability of O<sub>2</sub> to quench the excited state (13), and resistance of the chromophore to titration of the external pH (6). It also allows one to rationalize why fluorophore formation should be a spontaneous intramolecular process (8), because it is difficult to imagine how an enzyme could gain access to the substrate. The plane of the chromophore is roughly perpendicular (60°) to the symmetry axis of the surrounding barrel. One side of the chromophore faces an unexpectedly large cavity that occupies a volume of ~135 Å<sup>3</sup> (14). The cavity does not open out to bulk solvent. Four water molecules are located in the cavity, forming a chain of hydrogen bonds linking the buried side chains of Gln<sup>222</sup> and Gln<sup>69</sup>. Unless occupied, such a large cavity would be expected to destabilize the protein by several kilocalories per mole (15). Part of the volume of the cavity might be the consequence of the compaction resulting from cyclization and de-

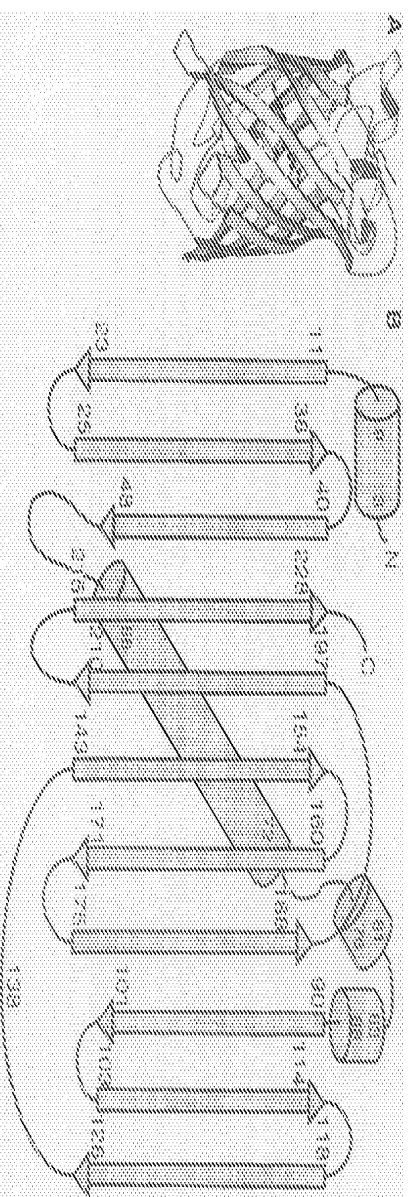


**Fig. 1. (A)** Schematic drawing of the backbone of GFP produced by the program MOLSCRIPT (32). The chromophore is shown as a ball and stick model. **(B)** Schematic drawing of the overall fold of GFP. Approximate residue numbers mark the beginning and ending of the secondary structure elements. N, NH<sub>2</sub>-terminus; C, COOH-terminus.

hydration reactions. The cavity might also temporarily accommodate the oxidant, most likely O<sub>2</sub> (4, 8, 16), that dehydrogenates the α-β bond of Tyr<sup>66</sup>. The chromophore, cavity, and side chains that contact the chromophore are shown in Fig. 2A, and a portion of the final electron density map in this vicinity is shown in Fig. 2B. The opposite side of the chromophore is packed against several aromatic and polar side chains. Of particular interest is the intricate network of polar interactions with the chromophore (Fig. 2C). His<sup>148</sup>, Thr<sup>203</sup>, and Ser<sup>205</sup> form hydrogen bonds with the phenolic hydroxyl; Arg<sup>96</sup> and Gln<sup>94</sup> interact with the carbonyl of the imidazolidinone ring, and Glu<sup>222</sup> forms a hydrogen bond with the side chain of Thr<sup>65</sup>. Additional polar interactions, such as hydrogen bonds to Arg<sup>96</sup> from the carbonyl of Thr<sup>62</sup>, and the side-chain carbonyl of Gln<sup>183</sup>, presumably stabilize the buried Arg<sup>96</sup> in its protonated form. In turn, this buried charge suggests that a partial negative charge resides on the carbonyl oxygen of the imidazolidinone ring of the deprotonated fluorophore, as has previously been suggested (6). Arg<sup>96</sup> is likely to be essential for the formation of the fluorophore and may help catalyze the initial ring closure. Finally, Tyr<sup>145</sup> shows a typical stabilizing edge-face interaction with the benzyl ring. Trp<sup>57</sup>, the only tryptophan in GFP, is located 13 to 15 Å from the chromophore, and the long axes of the two ring systems are nearly parallel. This conformation indicates that efficient energy transfer to the latter should occur and explains why no separate tryptophan emission is observable (2, 17).

Although the electron density map is for the most part consistent with the proposed structure of the chromophore (2, 7) in the *cis* [2-1] configuration, with no evidence for any substantial fraction of the opposite isomer around the chromophore double bond, difference features are found at  $>4\sigma$  in the final ( $F_o - F_c$ ) electron density map that can be interpreted to represent either the intact, uncyclized polypeptide or a carbinolamine (Fig. 2C, inset). This interpretation suggests that a significant fraction, perhaps as much as 30% of the molecules in the crystal, has failed to undergo the final dehydration reaction. Confirmation of incomplete dehydration comes from electrospray mass spectrometry, which consistently shows that the average masses of both wild-type and S65T GFP (31,086 ± 4 and 31,099.5 ± 4 daltons, respectively) are 6 to 7 daltons higher than predicted (31,079 and 31,093 daltons, respectively) for the fully matured proteins. Such a discrepancy could be explained by a 30 to 35% mole fraction of apoprotein or carbinolamine with 18 or 20 daltons higher molecular size (18). Mutants of GFP that increase the efficiency of fluorophore matu-

**Table 1.** Summary of GFP structure determination. Data were collected at room temperature in-house with either Molecular Structure Corporation R-axis II or San Diego Multiwire Systems (SDMS) detectors (Cu Kα) and later at beamline X4A at the Brookhaven National Laboratory at the selenium absorption edge (λ = 0.979 Å) with image plates. Data were evaluated by use of the HKL package (25) or the SDMS software (26). Each data set was collected from a single crystal. Heavy-atom soaks were 2 mM in mother liquor for 2 days. Initial electron density maps were based on three heavy-atom derivatives with the use of in-house data, then later were replaced with the synchrotron data. The EMTS (ethylmercurithiosalicylate) difference Patterson map was solved by inspection, then used to calculate difference Fourier maps of the other derivatives. Lack of closure refinement of the heavy-atom parameters was performed with the Protein package (27). The multiple isomorphous replacement (MIR) maps were much poorer than the overall figure of merit would suggest, and it was apparent that the EMTS isomorphous differences dominated the phasing. The enhanced anomalous occupancy for the synchrotron data provided a partial solution to the problem. The phasing power was reduced for the synchrotron data, but the figure of merit was unchanged. All experimental electron density maps were improved by solvent flattening with the program DM of the CCP4 (28) package, assuming a solvent content of 38%. Phase combination was performed with PHASCO2 of the Protein package with a weight of 1.0 on the atomic model. Heavy-atom parameters were subsequently improved by refinement against combined phases. Model building proceeded with FRODO and O (29), and crystallographic refinement was performed with the TNT package (30). Bond lengths and angles for the chromophore were estimated with CHEM3D (Cambridge Scientific Computing). Final refinement and model building were performed against the X4A selenium-edge data set, with (2F<sub>o</sub> - F<sub>c</sub>) electron density maps. The data beyond 1.9 Å resolution have not been used at this stage. The final model contains residues 2 to 229 as the terminal residues are not visible in the electron density map, and the side chains of several disordered surface residues have been omitted. Density is weak for residues 156 to 158, and coordinates for these residues are unreliable. This disordering is consistent with previous analyses showing that residues 1 and 233 to 238 are dispensable but that further truncations prevent fluorescence (12). The atomic model has been deposited in the Protein Data Bank (access code 1EMA).

Crystal	Resolution (Å)	Total observed	Unique observed	Compl. (%) <sup>*</sup>	Compl. (shell) <sup>†</sup>	R <sub>merge</sub> (%) <sup>‡</sup>	R <sub>iso</sub> (%) <sup>§</sup>
Diffraction data statistics							
<i>R-axis II</i>							
Native	2.0	51,907	13,582	80	69	4.1	5.8
EMTS <sup>  </sup>	2.6	17,727	6,787	87	87	5.7	20.6
SeMet	2.3	44,975	10,292	92	88	10.2	9.3
Multiwire							
HG14-Se	3.0	15,380	4,332	84	79	7.2	28.8
X4a							
SeMet	1.8	126,078	19,503	80	55	9.3	9.4
EMTS	2.3	57,812	9,204	82	66	7.2	26.3
Derivative	Resolution (Å)	Number of sites	Phasing power <sup>††</sup>	Phasing power (shell)	FOM <sup>¶</sup>	FOM (shell)	
Phasing statistics							
In-house							
EMTS	3.0	2	2.08	2.08	0.77	0.72	
SeMet	3.0	4	1.66	1.28	—	—	
HG14-Se	3.0	9	1.77	1.90	—	—	
X4a							
EMTS	3.0	2	1.36	1.26	0.77	0.72	
SeMet	3.0	4	1.31	1.08	—	—	
Atomic model statistics							
Protein atoms							1,790
Solvent atoms							94
Resolution range (Å)							20–1.9
Number of reflections ( <i>F</i> > 0)							17,676
Completeness							84
<i>R</i> factor <sup>**</sup>							0.175
Mean <i>B</i> value (Å <sup>2</sup> )							24.1
Deviations from ideality							
Bond lengths (Å)							0.014
Bond angles (°)							1.9
Restrained <i>B</i> values (Å <sup>2</sup> )							4.3
Ramachandran outliers							0

\*Completeness is the ratio of observed reflections to theoretically possible reflections expressed as a percentage. †Shell indicates the highest resolution shell, typically 0.1 to 0.4 Å wide. ‡ $R_{\text{merge}} = \sum |I - \langle I \rangle| / \sum I$ , where  $\langle I \rangle$  is the mean of individual observations of intensities. § $R_{\text{iso}} = \sum |F_o - F_c| / \sum F_o$ . ||Derivatives were EMTS (ethylmercurithiosalicylate; residues modified Cys<sup>94</sup> and Cys<sup>70</sup>), SeMet (selenomethionine-substituted protein; Met<sup>1</sup> and Met<sup>233</sup> could not be located), and HG14-SeMet (double derivative HG14 on a SeMet background). ¶Phasing power =  $(F_o - F_c) / (E)$ , where  $(F_o - F_c)$  is root mean square heavy-atom scattering and  $(E)$  is lack of closure. \*\*Standard figure of merit. \*\*Standard figure of merit.  $R = \sum |F_o - F_c| / \sum F_o$ .

rations might yield somewhat brighter preparations. In the model for the apoprotein (not shown), the Thr<sup>65</sup>-Tyr<sup>66</sup> peptide bond is approximately in the  $\alpha$ -helical conformation,

whereas the peptide of Tyr<sup>66</sup>-Gly<sup>67</sup> appears to be tipped almost perpendicular to the helix axis by its interaction with Arg<sup>96</sup>. This model further supports the possibility that

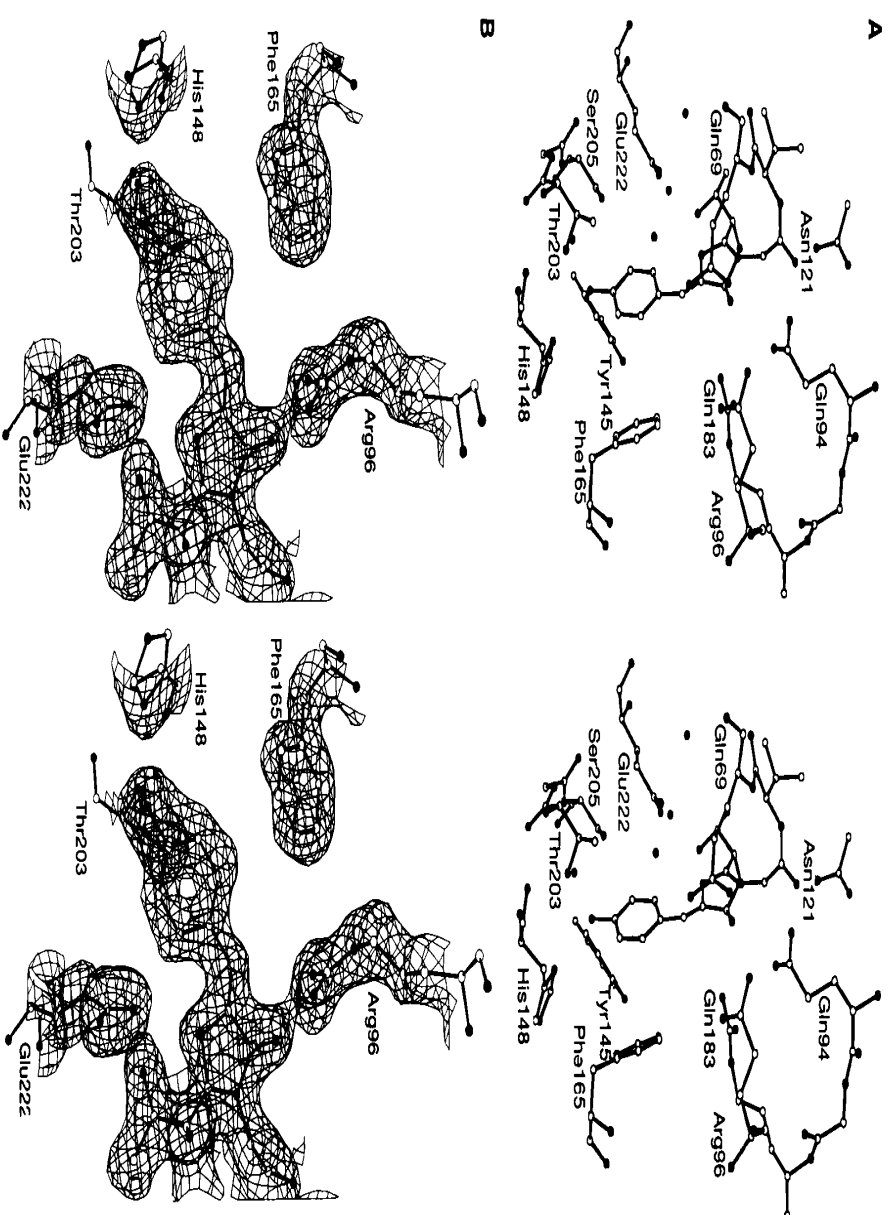
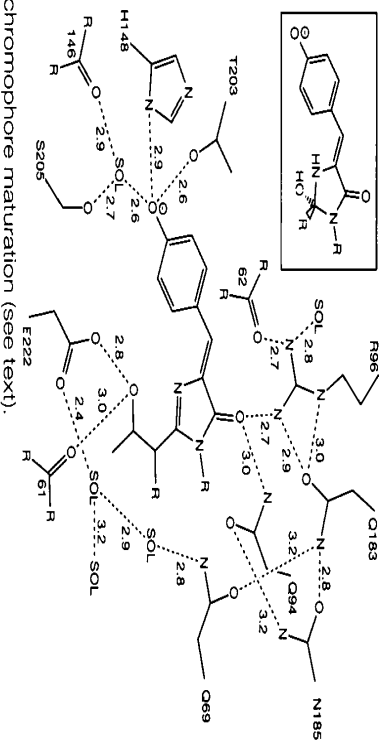


**Fig. 2. (A)** Stereo drawing of the chromophore and residues in the immediate vicinity. Carbon atoms are open circles, and oxygen atoms and nitrogen atoms are filled. Solvent molecules are shown as isolated filled circles. **(B)** Portion of the final  $2F_o - F_c$  electron density map contoured at  $1.0\sigma$ , showing the electron density surrounding the chromophore. **(C)** Schematic diagram showing the first and second spheres of coordination of the chromophore (9). Hydrogen bonds are shown as dashed lines and have the indicated lengths in Ångströms. (Inset) Proposed structure of the carbimolamine that may explain incomplete chromophore maturation (see text).



Arg<sup>96</sup> is important in generating the conformation required for cyclization, and possibly for promoting the attack of Gly<sup>67</sup> on the carbonyl carbon of Thr<sup>65</sup> (4).

The results of previous random mutagenesis studies have implicated several amino acid side chains in having substantial effects on the spectra, and the atomic model confirms that these residues are close to the chromophore. The mutations T203I and E222G have profound but opposite effects on the absorption spectrum (19). T203I (with wild-type Ser<sup>65</sup>) lacks the 475-nm absorbance peak usually attributed to the anionic chromophore and shows only the 395-nm peak thought to reflect the neutral chromophore (8, 19). Indeed, Thr<sup>203</sup> is hydrogen-bonded to the phenolic oxygen of the chromophore, so replacement by Ile should hinder ionization of the phenolic oxygen. Mutation of Glu<sup>222</sup> to Gly (19) has much the same spectroscopic effect as replacing Ser<sup>65</sup> by Gly, Ala, Cys, Val, or Thr, namely, suppression of the 395-nm peak in favor of a peak at 470 to 490 nm (10, 20). Indeed, Glu<sup>222</sup> and the remnant of Thr<sup>65</sup> are hydrogen-bonded to each other in the present structure, probably with the unchanged carbonyl of Glu<sup>222</sup> acting as donor to the side-chain oxygen of Thr<sup>65</sup>. Mutations E222G, S65G, S65A, and S65V would all suppress such hydrogen bonding. To explain why only wild-type protein has both excitation peaks, Ser<sup>65</sup>, unlike Thr<sup>65</sup>, may adopt a conformation in which its hydroxyl donates a hydrogen bond to and stabilizes Glu<sup>222</sup> as an anion, whose charge then inhibits ionization of the chromophore. The structure also explains why some mutations seem neutral. For example, Gln<sup>86</sup> is a surface residue far removed from the chromophore, which explains why its accidental and ubiquitous mutation to Arg seems to have no obvious intramolecular spectroscopic effect (3).

The development of GFP mutants with red-shifted excitation and emission maxima presents an interesting challenge in protein engineering (4, 10, 20). Such mutants would also be valuable for avoidance of cellular autofluorescence at short wavelengths, for simultaneous multicolor reporting of the activity of two or more cellular processes, and for exploitation of fluorescence resonance energy transfer as a signal of protein-protein interaction (21). Extensive studies with random mutagenesis have shifted the emission maximum by at most 6 nm to longer wavelengths (514 nm) (21); previously described "red-shifted" mutants merely suppressed the 395-nm excitation peak in favor of the 475-nm peak without any significant reddening of the 505-nm emission (20). Because Thr<sup>203</sup> is shown to be adjacent to the phenolic end of the chromophore, we mutated it to polar aromatic residues such as His, Tyr, and Trp in the hope that the additional polarizability of their  $\pi$

**Table 2.** Spectral properties of Thr<sup>203</sup> mutants compared to S65T (10). The mutations F64L, V68L, and S72A improve the folding of GFP at 37° (37) but do not significantly shift the emission spectra.

Clone	Mutations	Excitation maximum (nm)	Extinction coefficient (10 <sup>3</sup> M <sup>-1</sup> cm <sup>-1</sup> )	Emission maximum (nm)
S65T	S65T	489	39.2	511
5B.9B	T203H/S65T	513	19.4	524
6C	T203Y/S65T	513	14.5	525
10B	T203Y/F64L/S65G/S72A	513	30.8	525
10C	T203Y/S65G/V68L/S72A	513	36.5	527
11	T203W/S65G/S72A	502	33.0	512

systems would lower the energy of the excited state of the adjacent chromophore. All three substitutions did indeed shift the emission peak to >520 nm (Table 2). A particularly attractive mutation was T203Y/S65G/V68L/S72A, with excitation and emission peaks at 513 and 527 nm, respectively. These wavelengths are sufficiently different from those of previous GFP mutants to be readily distinguishable by appropriate filter sets on a fluorescence microscope. The extinction coefficient, 36,500 M<sup>-1</sup> cm<sup>-1</sup>, and quantum yield, 0.63, are almost as high as those of S65T (10).

Comparison of *Aequorea* GFP with other protein pigments is instructive. Unfortunately, its closest characterized homolog, the GFP from the sea pansy *Renilla reniformis* (1, 6), has not been sequenced or cloned, although its chromophore is derived from the same FSYG sequence as in wild-type *Aequorea* GFP (22). The closest analog for which a three-dimensional structure is available is the photoreceptor protein (PYP) (23), a 14-kD photoreceptor from halophilic bacteria. PYP in its native dark state absorbs maximally at 446 nm and transduces light with a quantum yield of 0.64, rather closely matching wild-type GFP's long-wavelength absorbance maximum near 475 nm and fluorescence quantum yield of 0.72 to 0.85. The fundamental chromophore in both proteins is an anionic *p*-hydroxynaphthyl group, which is covalently attached to the protein via a thioester linkage in PYP and a heterocyclic iminolactam in GFP. Both proteins stabilize the negative charge on the chromophore with the help of buried cationic arginine and neutral glutamic acid groups.

Arg<sup>52</sup> and Glu<sup>46</sup> in PYP and Arg<sup>96</sup> and Glu<sup>122</sup> in GFP, although in PYP the residues are close to the oxyphenyl ring whereas in GFP they are nearer the carbonyl end of the chromophore. However, PYP has an overall  $\alpha/\beta$  fold with appropriate flexibility and signal transduction domains to enable it to mediate the cellular phototactic response, whereas GFP has a much more regular and rigid  $\beta$  barrel to minimize parasitic dissipation of the excited state energy as thermal or conformational motions. GFP provides an elegant example of how a visually appealing and extremely useful function—efficient fluores-

cence—can be spontaneously generated from a cohesive and economical protein structure. *Note added in proof:* An independent determination of the structure of wild-type GFP has been carried out by Yang *et al.* (24).

## REFERENCES AND NOTES

- O. Shimomura and F. H. Johnson, *J. Cell. Comp. Physiol.*, **59**, 223 (1962); J. G. Morin and J. W. Hastings, *J. Cell. Physiol.*, **77**, 313 (1971); H. Morise, O. Shimomura, F. H. Johnson, J. Winant, *J. Biochem.*, **13**, 2656 (1974); W. W. Ward, *Photochem. Photobiol. Rev.*, **4**, 1 (1979).
- D. C. Prasher, V. K. Eckenrode, W. W. Ward, F. G. Prendergast, M. J. Cormier, *Gene*, **111**, 229 (1992).
- M. Chalfie, Y. Tu, G. Euskirchen, W. W. Ward, D. C. Prasher, *Science*, **263**, 802 (1994).
- A. B. Cubitt *et al.*, *Trends Biochem. Sci.*, **20**, 448 (1995).
- D. C. Prasher, *Trends Genet.*, **11**, 320 (1995); M. Chalfie, *Photochem. Photobiol.*, **62**, 651 (1995).
- W. W. Ward, in *Bioluminescence and Chemiluminescence*, M. A. Deluca and W. D. McElroy, Eds. (Academic Press, New York, 1981), pp. 235–242; and S. H. Bokman, *Biochemistry*, **21**, 4535 (1982); W. W. Ward *et al.*, *Photochem. Photobiol.*, **35**, 803 (1982).
- C. W. Cody, D. C. Prasher, W. M. Westler, F. G. Prendergast, W. W. Ward, *Biochemistry*, **32**, 1212 (1993).
- R. Heim, D. C. Prasher, R. Y. Tsien, *Proc. Natl. Acad. Sci. U.S.A.*, **91**, 12501 (1994).
- Abbreviations for the amino acid residues are as follows: A, Ala; C, Cys; D, Asp; E, Glu; F, Phe; G, Gly; H, His; I, Ile; K, Lys; L, Leu; M, Met; N, Asn; P, Pro; Q, Gln; R, Arg; S, Ser; T, Thr; V, Val; W, Trp; and Y, Tyr.
- R. Heim, A. B. Cubitt, R. Y. Tsien, *Nature*, **373**, 664 (1995).
- This mutant also contains the ubiquitous O80R substitution, which accidentally occurred in the early distribution of the GFP cDNA and is not known to have any effect on the protein properties (3). Histidine-tagged S65T GFP (10) was overexpressed in the plasmid JM109/PRSETg in 4 liters of YT broth plus ampicillin at 37°C, stirred at 450 rpm and 5 liter/min air flow. The temperature was reduced to 25°C at an absorbance at 595 nm ( $A_{595}$ ) of 0.3, followed by induction with 1 mM isopropyl- $\beta$ -thiogalactoside for 5 hours. Cell paste was stored at –80°C overnight and then resuspended in 50 mM Hepes (pH 7.9), 0.3 M NaCl, 5 mM 2-mercaptoethanol, 0.1 mM phenylmethylsulfonyl fluoride (PMSF), passed once through a French press at 68,000 kPa, then centrifuged at 48,400g for 45 min. The supernatant was applied to a Ni-nitrilotriacetic acid (NTA) agarose column (Qiagen), followed by washing with 20 mM imidazole, then eluted with 100 mM imidazole. Green fractions were pooled and subjected to chromatography (Sigma) proteolysis (1:50 w/w) for 22 hours at room temperature. After addition of 0.5 mM PMSF, the digest was reapplied to the Ni column. NH<sub>4</sub>-terminal sequencing verified the presence of the correct NH<sub>2</sub>-terminal methionine. After dialysis against 20 mM Hepes (pH 7.5) and concentration to  $A_{280} = 20$ , rod-shaped crystals were obtained at room temperature in hanging drops containing 5  $\mu$ l of protein and 5  $\mu$ l of well solution, 22 to 26% polyethylene glycol (PEG 4000, Serva), 50 mM Hepes (pH 8.0 to 8.5), 50 mM MgCl<sub>2</sub>, and 10 mM 2-mercaptoethanol within 5 days. Crystals were 0.05 mm across and up to 1.0 mm long. The space group is P2<sub>1</sub>2<sub>1</sub>2<sub>1</sub>, with  $a = 51.8$ ,  $b = 62.8$ ,  $c = 70.7$  Å,  $Z = 4$ . Two crystal forms of wild-type GFP, unrelated to the present form, have been described by M. A. Perrozo, K. B. Ward, R. B. Thompson, and W. W. Ward [*J. Biol. Chem.*, **263**, 7713 (1988)].
- J. Dopf and T. M. Horstgen, *Gene*, **173**, 39 (1996).
- B. D. Nagaswara Rao, M. D. Kempe, F. G. Prendergast, *Biophys. J.*, **32**, 630 (1980).
- B. Lee and F. M. Richards, *J. Mol. Biol.*, **55**, 379 (1971). The atomic radii were those of Lee and Richards, calculated by use of the program MS with a probe radius of 1.4 Å [M. L. Connolly, *Science*, **221**, 709 (1983)].
- S. J. Hubbard, K.-H. Gross, P. Argos, *Protein Eng.*, **7**, 613 (1994); A. E. Eriksson *et al.*, *Science*, **265**, 178 (1992).
- S. Inouye and F. I. Tsui, *FEBS Lett.*, **351**, 211 (1994).
- The two cysteines in GFP, Cys<sup>65</sup> and Cys<sup>70</sup>, are 24 Å apart, too distant to form a disulfide bridge. Cys<sup>70</sup> is buried, but Cys<sup>65</sup> should be relatively accessible to sulphydryl-specific reagents. Such a reagent, 5,5'-di-thiobis(2-nitrobenzoic acid), is reported to label GFP and quench its fluorescence (16). This effect was attributed to the necessity for a free sulphydryl, but could also reflect specific quenching by the 5'-thio-2-nitrobenzoate moiety that would be attached to Cys<sup>65</sup>.
- The natural abundance of <sup>13</sup>C and <sup>2</sup>H and the finite resolution of the Hewlett-Packard 5989B electrospray mass spectrometer used to make these measurements do not permit the individual peaks to be resolved, but instead yield an average mass peak with a full width at half maximum of 55 daltons. The molecular sizes shown include the His-tag, which has the sequence MRGSH-HH-HGMSMTG-GGGMGRDLYDDDKDPAAEF (9, 10).
- T. Enrig, D. J. O'Kane, F. G. Prendergast, *FEBS Lett.*, **367**, 163 (1995).
- S. Delagrave, R. E. Hawtin, C. M. Silva, M. M. Yang, D. C. Youvan, *Bio/Technology*, **13**, 151 (1995).
- R. Heim and R. Y. Tsien, *Curr. Biol.*, **6**, 178 (1996).
- R. M. San Pietro, F. G. Prendergast, W. W. Ward, *Photochem. Photobiol.*, **57**, 563 (1993).
- G. E. O. Borgstahl, D. R. Williams, E. D. Getzoff, *Biochemistry*, **34**, 6278 (1995).
- F. Yang, L. G. Moss, G. N. Phillips, *Nature Biotechnol.*, in press.
- Z. Otwinowski, in *Proceedings of the CCP4 Study Weekend: Data Collection and Processing*, L. Sawyer, N. Isaacs, S. Bailey, Eds. (Science and Engineering Research Council, Daresbury Laboratory, Warrington, UK, 1991), pp. 56–62; W. Minor, XDISPLAY (Purdue University, West Lafayette, IN, 1993).
- A. J. Howard, C. Nielsen, N. H. Xuong, *Methods Enzymol.*, **114**, 452 (1985).
- W. Steigemann, thesis, Technical University, Munich (1974).
- CCP4: A Suite of Programs for Protein Crystallography (Science and Engineering Research Council, Daresbury Laboratory, Warrington, UK, 1979).
- T. A. Jones, J.-Y. Zou, S. W. Cowan, M. Kjeldgaard, *Acta Crystallogr. Sect. A*, **47**, 110 (1991); T. A. Jones, in *Computational Crystallography*, D. Sayre, Ed. (Oxford Univ. Press, Oxford, 1992), pp. 303–317.
- D. E. Tronrud, L. F. Ten Eyck, B. W. Matthews, *Acta Crystallogr. Sect. A*, **43**, 489 (1987).
- B. P. Cormack, R. H. Valdivia, S. Falkow, *Gene*, **173**, 33 (1996).
- P. J. Kraulis, *J. Appl. Crystallogr.*, **24**, 946 (1991).
- We thank T. Ross for initial crystallization of GFP, M. Sagermann for help with the CCP4 package for crystallographic computing, and M. Elsinger, C. Ogata, and R. Brennan for help with data collection. Facilities at the University of Oregon and beamline X4A at the Brookhaven National Laboratory are supported in part by the Howard Hughes Medical Institute and a grant from the National Science Foundation (MCB 9418479) to S.J.R. M.O. gratefully acknowledges the Swedish Natural Science Research Council for a postdoctoral fellowship.